

**SIMULATING COLLISIONAL DARK
MATTER USING A LATTICE
BOLTZMANN METHOD**

**Javier Alejandro
Acevedo Barroso**

Advisor:
Dr. Jaime E. Forero-Romero

A monograph presented for the degree of Physicist



Departamento de Física
Facultad de Ciencias
Universidad de los Andes
Bogotá, Colombia

November, 2018

*Dedicado a
Satán*

Contents

1	Introduction	1
1.1	General objective	2
1.2	Specific objectives	2
1.3	Dark Matter	3
1.3.1	The Cluster Missing Mass Problem	3
1.3.2	Galaxy Rotation Curves	5
1.3.3	The Bullet Cluster	7
1.4	The Boltzmann Equation	9
1.5	Lattice Boltzmann Method	10
1.6	BGK Approximation	11
2	The Lattice Boltzmann Algorithm	13
2.1	General Description	13
2.2	The Collisional Step	18
2.2.1	Units on the simulation	22
3	Results	23
3.1	The two dimensional phase space	24

CONTENTS

3.1.1	No collisional case	25
3.1.2	The collisional case	33
3.2	Four dimensional phase space	35
3.2.1	No collisional case	36
3.3	Six dimensional phase space	37
4	Conclusions	38
4.1	A Numerically Stable Simulation	38

List of Figures

1.1	A comparison between the model from photometrical measurements and the curves measured. This curves are illustrative and do not correspond to a particular galaxy.	6
2.1	Flowchart of the algorithm.	15
3.1	Up: initialization of the phase space. Position is represented in the x axis, and velocity in the y axis of the plot. Down: the spatial density obtained through integration.	26
3.2	Up: The potential obtained by solving the Poisson equation. Given that the density was a Gaussian profile, it is no surprise that the potential is a negative Gaussian profile. Down: The acceleration obtain by numerical derivation of the potential.	27
3.3	Upper left: Phase space 72 million years after initialization. Upper right: Phase space 227 million years after initialization. Bottom left: Phase space 413 million years after initialization. Bottom right: Phase space 930 million years after initialization. It can be observed that the phase space behaves as a clock-wise rotating spiral.	28

LIST OF FIGURES

3.4	Upper left: linear density with its central peak at maximum height. Upper right: linear density the peak at a local minima after having reached maximum height . Bottom left: little bumps can be seen at the tails of the distribution. Bottom right: the tails of the distribution are completely bumpy and so is the base of the peak. The images are from 31, 114, 300 and 920 million years after initialization.	29
3.5	Upper left: Phase space 72 million years after initialization. Upper right: Phase space 227 million years after initialization. Bottom left: Phase space 413 million years after initialization. Bottom right: Phase space 930 million years after initialization. The behavior is the same as three successive Gaussian conditions.	31
3.6	Upper left: phase space initialization of the <i>Bullet Cluster</i> run. The right halo is slightly less massive (dimmer). Upper right: phase space during the spatial collision of the halos. The gap in the velocity axis keeps the halos decoupled. Bottom left: phase space with the position of the halos switched in regards of the centre of mass and the initial conditions. Bottom right: the system after a full period. The halos are at their initial position but their velocities have changed due to the evolution of each Gaussian.	33
3.7	Upper left: density initialization of the <i>Bullet Cluster</i> run. Notice that the left halo is heavier. Upper right: density during the spa- tial collision of the halos. Bottom left: density when the halos have switched position with regards to the centre of mass. Bottom right: the system after a full period. The halos are at their initial position but their velocities have changed.	34

3.8 Upper left: density initialization of the <i>Bullet Cluster</i> run. Notice that the left halo is heavier. Upper right: density during the spatial collision of the halos. Bottom left: density when the halos have switched position with regards to the centre of mass. Bottom right: the system after a full period. The halos are at their initial position but their velocities have changed.	35
--	----

Chapter 1

Introduction

Traditionally, dark matter has been simulated by using N-body schemes, in which the temporal evolution of a system of N particles is simulated usually by solving the Poisson-Vlasov equation [1]. These N-body simulations have been essential for the development of modern cosmology and the characterization of dark matter halos. For example, the development of the Λ CMD cosmology was heavily linked with a classic N-body simulation of the large scale structure of the universe which used only 32748 particles! [2].

On the other hand, Lattice-Boltzmann simulations have been widely used to simulate increasingly complex fluids and boundary conditions, nonetheless, the usual Lattice-Boltzmann scheme does not simulate the entire velocity space, but simply a small number of adventive velocities.

Inspired by the work of Philip Mocz, Sauro Succi [3], and Sebastian Franco [4], in which a Lattice-Boltzmann simulation is used to simulate the phase space of a

1.1. GENERAL OBJETIVE

collisionless one dimensional dark matter fluid. We implement a Lattice-Boltzmann simulation of the phase space of a *collisional* three dimensional dark matter fluid using the BGK approximation for the collisional term.

1.1 General objetive

To simulate the phase space of a collisional dark matter fluid using a Lattice-Boltzmann method.

1.2 Specific objetives

- To implement a Lattice-Boltzmann simulation using a 4-dimensional phase space and a varying collisional term.
- To implement a Lattice-Boltzmann simulation using a 6-dimensional phase space and a varying collisional term.
- To study the dynamical behavior of a dark matter fluid using different equilibrium distributions in the collisional term.
- To simulate the phase space of a collisional dark matter fluid using literature values for the thermally averaged cross-section and compare it with its collisionless version.

In order to follow the ideas and developments of the upcoming chapters, it is essential to understand some concepts and computational techniques. In this chapter, we present all the necessary knowledge for the proper understanding of this work.

1.3 Dark Matter

Modern cosmology describes the universe as being composed of two fundamental types of energy: dark energy and matter¹, with dark energy being associate with a cosmological constant and matter being divided into two categories: dark matter and standard model matter². The energy density of the universe is 69% dark energy and 31% matter[5].

Standard model matter includes all the particles whose interactions can be properly described by the standard model, such as: Protons, Electrons, Atoms and naturally, any structure that they form, like humans or stars. On the other hand, dark matter is all the matter we measure from astrophysical sources which cannot be explained by baryonic matter. We know of the existence of dark matter entirely from astrophysical evidence, during this section we are going to do an historical review of such evidence.

1.3.1 The Cluster Missing Mass Problem

The traditional history of dark matter begins in the 1930s with the swiss astronomer Fritz Zwicky[6] [7], who noticed an unusually high velocity dispersion between the

¹In relativity, mass and energy are equivalent.

²Which often is called “Baryonic matter” due to Baryons being the largest fraction of this mass.

1.3. DARK MATTER

galaxies of the Coma Cluster. To tackle the problem, Zwicky assumed that the Coma Cluster “had already reached a mechanically stationary state” [8] and such, the virial theorem could be applied. By counting galaxies, along with assuming that matter is distributed uniformly in the cluster and using Hubble’s estimate of the mean mass of a galaxy, Zwicky was able to estimate the potential energy of the Cluster. Using his estimate of the visible mass and the virial theorem, Zwicky concluded that the velocity dispersion must be $\sqrt{v^2} = 80$ km/s. Nonetheless, the real measurement of the velocity dispersion was $\sqrt{v^2} = 1000$ km/s, implying a virial mass about 400 times larger than the visible mass³. Zwicky called the discrepancy between the luminous matter (in the form of visible galaxies which could simply be counted) and the virial matter (obtained from the virial theorem and the high velocity dispersion of the cluster) “Dark Matter”.

By the late 1950s similar calculations for different clusters had been published. Many of those calculations had very large values for the mass-to-light ratio[9], which were consistent with the mass-to-light ratio calculated from the Coma Cluster. The problem of the missing mass seemed to appear in almost every large scale structure in the universe, and by the early 1970s astrophysicist had already disregarded hot gas[10] and free hydrogen[11] as explanations for the missing mass in Clusters. Nonetheless, it was still possible that the missing mass problem could be in fact solved by a more refined model of the cluster kinematics, because so far, the missing mass problem had only been observed on Clusters and large scale structures.

³This ratio is often called the mass-to-light ratio.

1.3.2 Galaxy Rotation Curves

A galaxy rotation curve plots the orbital velocity of stars in a galaxy versus their distance to the galaxy centre. These curves became very informative thanks to the work of the Indian astrophysics Subrahmanyan Chandrasekhar, who proved that the mutual interactions between stars were negligible, so a galaxy could be modeled as a non-interacting system of stars [12]. Such modeling allows to obtain mass profiles from galaxy rotation curves. Now, due to photometric measurements, astrophysicist believed that most of galaxy's mass was overwhelmingly concentrated in the galaxy centre, therefore, it was reasonable to model the galaxy similarly to the solar system.

Consider a star in the galaxy disk with mass m at a distance r from the galaxy centre. Given that we can disregard the interaction between starts, the sum of forces acting on the object is simply the gravitational attraction towards the galaxy centre:

$$m \frac{v^2}{r} = G \frac{mM}{r^2} \quad (1.1)$$

With M being the mass enclosed by the star orbit and v being the orbital velocity of the star. Finally, the galaxy rotation curve for such galaxy will be given by:

$$v(r) = \sqrt{\frac{GM}{r}} \quad (1.2)$$

Which means that for objects outside of the galaxy disk (but still under the influence of the galaxy gravitational pull) the enclosed mass will be constant regardless of the radius, and thus, the orbital velocity will be proportional to $r^{-1/2}$. With the advent of radio astronomy and the invention of the Image Tube Spectrograph, astronomers were able to measure orbital velocities way beyond the apparent end of the luminous

1.3. DARK MATTER

galaxy disks, only to find that the orbital velocity did not decay proportionally to $r^{-1/2}$ but it stayed more or less constant[13] [14] [15]. This behavior can be seen easily in the figure 1.1:

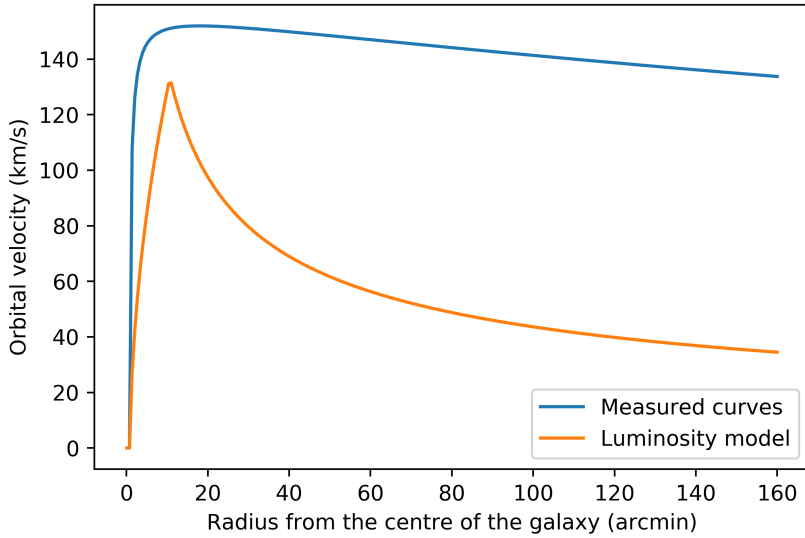


Figure 1.1: A comparison between the model from photometrical measurements and the curves measured. These curves are illustrative and do not correspond to a particular galaxy.

This unexpected velocity profile implied a mass-to-light ratio that increased with distance and also the existence of mass beyond the visible galactic disk[16]. The overwhelming amount of high quality galaxy rotation curves measurements, led to the acceptance of the dark matter hypothesis in the astrophysical community.

Throughout the use of numerical simulations and the measurement of more galaxy rotation curves during the 1980s and the 1990s, it was concluded that the dark matter density in galaxies was well modeled by the Navarro-Frenk-White (NFW)

profile[17][18]

$$\rho(r) = \frac{\rho_0}{r/r_s(1+r/r_s)^2} \quad (1.3)$$

1.3.3 The Bullet Cluster

Galaxy clusters have three main constituents: dark matter, intracluster gas (which is mostly ionised hydrogen and helium), and the galaxy themselves.[19]

We can observe the intracluster baryonic matter in the x-ray band thanks to Bremsstrahlung radiation, therefore, by doing photometry in X-ray it is possible to map the baryonic gas distribution in a cluster. In the case of dark matter, we infer its existence in clusters thanks to the work of Fritz Zwicky and the posterior work in the missing mass problem in galaxy clusters. Our current estimates place most of the cluster mass in the dark matter component. By analyzing the gravitational lensing effect (in particular the *weak* gravitational lensing effect) it is possible to map the mass distribution of a galaxy cluster. Lastly, we can observe the galaxies in the visual and the infrared band. They are the only component of a galaxy cluster that can be observed in the visual band. About 90 percent of the mass of a cluster is dark matter (this is not a surprise since Fritz Zwicky measured mass-to-light ratios of 50 during the 1930s). Of the remaining baryonic matter, the ionized gas mass can represent up to 90% of the mass, making galaxies responsible of about 1% of the total cluster mass.

The object Bullet Cluster (also known as 1E 0657-558) is the aftermath of the collision of two galaxy cluster. Before the collision, each cluster had its own set galaxies, baryonic gas and dark matter, and the centroid of each constituent coincided with

1.3. DARK MATTER

the center of mass of the whole cluster. During the collision, each constituent reacts differently to the situation:

- Galaxies, given that they occupy a minuscule fraction of the total volume of the cluster, are essentially collisionless. Two galaxy clusters can collide without any galaxy (or very little galaxies) colliding per se.
- Dark matter is also modeled as collisionless, therefore, during the collision of two galaxy clusters, the dark matter components simply pass through, similarly to how Neutrinos constantly cross the Earth without losing a significant amount of energy.
- The baryonic gas on the other hand is collisional, and its short range interactions are very well described by the Standard Particle Model. During the galaxy cluster collision, the baryonic parts interact and they lose energy through particle collision. This interaction decouples the baryonic gas from the galaxies and dark matter, and, given that we can directly observe the hot gas (thanks to X-ray astronomy), we can measure the separation between the centroid of the hot gas and the centroid of the galaxies.

If there was no dark matter, then after the collision the weak lensing mapping of the mass distribution would be very close to the hot gas distribution, because the hot gas would be the dominant mass density in the cluster. If dark matter were to exists, then it would dominate the mass density distribution in the galaxy cluster and the weak lensing mapping would be very similar to the galaxies distribution (because they are also collisionless).

What we observe in the Bullet Cluster is the latter case, in which hot gas decouples

from dark matter and galaxies. By mapping the cluster components and measuring the difference between the centroids, it was concluded that there is a dark matter component in the clusters. Very accurate measurements and estimates of the centroids show a small collisional nature in the dark matter component, such measurements allows estimate the *thermally averaged cross-section* of the dark matter particle ($\langle \sigma v \rangle$). Therefore, it is worth exploring the collisional dark matter scenario.

1.4 The Boltzmann Equation

The Boltzmann equation was originally proposed in 1872 by Ludwig Boltzmann and is used to model the behavior of statistical systems outside of the equilibrium. Formally, the Boltzmann equation describes the evolution of the phase space of a typical dark matter particle, such that $f(\mathbf{r}, \mathbf{v}, t)d\mathbf{r}d\mathbf{v}$ is the probability of finding the dark matter particle in a position between \mathbf{r} and $\mathbf{r}+d\mathbf{r}$, with velocity between \mathbf{v} and $\mathbf{v} + d\mathbf{v}$. Given than a halo is made of typical dark matter particles, we can treat it as a dark matter fluid and apply the Boltzmann equation now interpreting $f(\mathbf{r}, \mathbf{v}, t)d\mathbf{r}d\mathbf{v}$ as the number of dark matter particles whose position is between \mathbf{r} and $\mathbf{r} + d\mathbf{r}$ with velocity between \mathbf{v} and $\mathbf{v} + d\mathbf{v}$. Regardless of whether we are thinking of a fluid or a particle, the Boltzmann equation is given by:

$$\frac{\partial f}{\partial t} + \dot{\mathbf{x}} \frac{\partial f}{\partial \mathbf{x}} + \dot{\mathbf{v}} \frac{\partial f}{\partial \mathbf{v}} = C[f] \quad (1.4)$$

The left hand side is known as the Liouville operator and the right hand side is

known as the *Collisional* operator. The Liouville operator represents the evolution of the system followed classical mechanics, without considering short range interaction between particles (the collisions). The collisional operator is an integral operator that relates the possibility of a collision with the state of the system $f(\mathbf{r}, \mathbf{v}, t)$. In other words, the collisional operator quantifies the effect of the collisions in the phase space evolution. A complete modeling of the collisional operator requires knowledge of the short range interactions between particles, given that we do not know the short range interaction of a dark matter particle, we must work with approximation schemes. This is going to be expanded in [1.6](#).

For a collisionless fluid, the Boltzmann equation becomes the Vlasov equation:

$$\frac{\partial f}{\partial t} + \dot{\mathbf{x}} \frac{\partial f}{\partial \mathbf{x}} + \dot{\mathbf{v}} \frac{\partial f}{\partial \mathbf{v}} = 0 \quad (1.5)$$

Which simply dictates that the phase space distribution function is constant along the trajectories of the system[\[3\]](#)

1.5 Lattice Boltzmann Method

The Lattice-Boltzmann method consists of dividing the phase space into a lattice and solving the Boltzmann equation in such lattice. In each unit of the lattice there is a density which represents the amount of fluid in the position and velocity range correspondent to the cell's location in the lattice. The main effect of the discretization of the phase space is that we no longer simulate the entire phase space, but a countable number of velocities and positions, which allows for the use of

integer arithmetic when updating the lattice. The use of integer arithmetic introduces a lattice noise but eliminates the floating point error. In the limit of high resolution, the absence of floating point error and the tendency of the lattice noise towards zero guarantees that the method converges to the continuum solution and makes it a Lagragian, Symplectic and conservative algorithm.

However, this method has one big drawback. The time evolution of the phase space is calculated using a direct integration scheme, which implies that for a simulation with N spatial dimensions each one having size n , we would need to store n^{2N} cell units per timestep. This is in fact a very heavy constrain because most cases of interest are three dimensional. For example, consider a three dimensional dark matter halo, if the grid size were to be 64, then we would need almost 600 Gigabytes of memory just to store the lattice!

The specifics of implementing a Lattice Boltzmann method is discussed further in section 2.1

1.6 BGK Approximation

The main challenge when solving the Boltzmann equation is the collisional operator. Modeling a collisional operator and solving the subsequent integral is not a straightforward procedure, which is why simpler alternatives have been widely considered.

The Bhatnagar–Gross–Krook approximation was proposed in 1954 [20] in order to simplify the collision integral. The approximation operates under the assumption that the large amount of detail involved in the two-body interactions are not likely

1.6. BGK APPROXIMATION

to significantly influence the macroscopic variables[21]. This is known as an mesoscopic approach, because we disregard the microscopic interactions but preserving the macroscopic properties of the system. The scheme ignores the specifics of the two-body interactions but keeps the tendency of the system towards local equilibrium and then towards global equilibrium.

Local equilibrium is defined by the condition:

$$C[f_e] = 0 \quad (1.6)$$

Which simply states that in *local equilibrium*, the collisions do not affect the time derivative of the distribution function. Note that local equilibrium does not mean that the macroscopic variables of the system are constant in space and time, but that the local value of $f(\mathbf{r}, \mathbf{v}, t)$ corresponds to the local value of $f_e(\mathbf{r}, \mathbf{v})$, for an appropriate equilibrium distribution function $f(\mathbf{r}, \mathbf{v})$. Finally, the BGK operator can be stated as:

$$C[f] = -\frac{1}{\tau}(f(\mathbf{r}, \mathbf{v}, t) - f_e(\mathbf{r}, \mathbf{v})) \quad (1.7)$$

Where τ is a characteristic relaxation time for the system. In most cases, the equilibrium function obeys the Maxwell-Boltzmann distribution, nonetheless, Fermi-Dirac distributions were widely used in the early years of the Lattice Boltzmann methods. In recent years modified Maxwellians have been proposed to extend the BGK scheme to the quantum realm[22] and to include annihilation and creation of particles. The specifics of our implementation of the BGK approximation are discussed in section [2.2](#).

Chapter 2

The Lattice Boltzmann Algorithm

2.1 General Description

Now that we have overviewed the pertinent concepts, we can proceed to the particulars of this implementation. As previously asserted, the heart of the Lattice-Boltzmann Algorithm lies on its discretization of the phase space[4] [3].

To discretize the phase space, we must choose the region to simulate. In this work, we name the extremal values in the w axis of the phase space W_{min} and W_{max} . Then, one has to fix either the size of the grid or the size of the lattice. We name the size of the grid in the w axis N_w (i.e. N_x or N_{vz}). The size of the lattice in the w axis (which we are going to name dw) and the extremal values are related by:

$$dw = \frac{W_{max} - W_{min}}{N_w} \quad (2.1)$$

2.1. GENERAL DESCRIPTION

In this work we are going to use the phase-space mass *density*, which means that $f(\mathbf{r}, \mathbf{v}, t)d\mathbf{r}d\mathbf{v}$ is the density of dark matter whose position is between \mathbf{r} and $\mathbf{r} + d\mathbf{r}$, and its velocity is between \mathbf{v} and $\mathbf{v} + d\mathbf{v}$. Now that we have properly defined the phase space grid, we can proceed to initialization. For simplicity, we developed the simulation using Gaussian initial conditions given by:

$$f(\mathbf{r}, \mathbf{v}, 0) = A \exp \left\{ -\frac{\mathbf{r}^2}{\sigma_r^2} - \frac{\mathbf{v}^2}{\sigma_v^2} \right\} \quad (2.2)$$

Where $f(\mathbf{r}, \mathbf{v}, 0)$ is the initialization of the phase space density, A is an indirect measure of the total mass in the system, \mathbf{r} is the vector (x, y, z) , \mathbf{v} is the vector (vx, vy, vz) , and σ_i are a measure of the width of the Gaussian profile in the given axis. Note that we use a single width for the spatial axes (σ_r) and a single width for the velocity axes (σ_v). Alternative initialization distributions are going to be considered in the results chapter.

After initialization, the system evolves by the action of the Louville operator and the Collisional operator, nonetheless, the collisions are modeled as instant, which allows to concentrate they entire influence in a collisional step. The schematics of the algorithm can be seen easily in figure 2.1.

Now that we have defined the phase-space, we can obtain the spatial density of matter by integrating the phase space:

$$\rho(\mathbf{r}, t) = \int_{-\infty}^{\infty} f(\mathbf{r}, \mathbf{v}, t) d\mathbf{v}. \quad (2.3)$$

When evaluating in the lattice the integral becomes a sum over the entire velocity

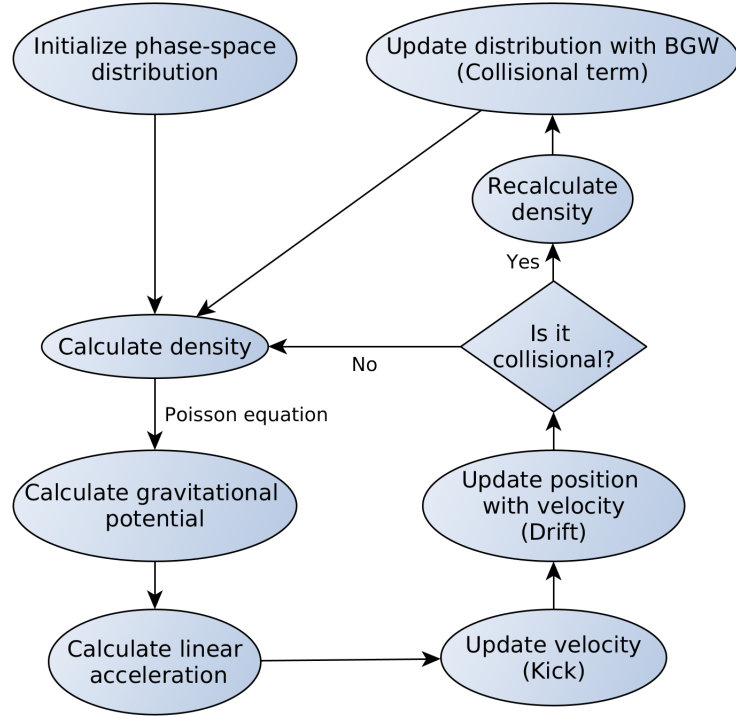


Figure 2.1: Flowchart of the algorithm.

lattice:

$$\rho(\mathbf{r}, t) = \sum_{\mathbf{v}_{min}}^{\mathbf{v}_{max}} f(\mathbf{r}, \mathbf{v}, t) d\mathbf{v} \quad (2.4)$$

and during initialization:

$$\rho(\mathbf{r}, 0) = \sum_{\mathbf{v}_{min}}^{\mathbf{v}_{max}} f(\mathbf{r}, \mathbf{v}, 0) d\mathbf{v} \quad (2.5)$$

Once we have calculated the density, we solve the Poisson equation to obtain the potential due to gravitational interaction: [3]

$$\nabla^2 \Phi(\mathbf{r}, t) = 4\pi G \rho(\mathbf{r}, t) \quad (2.6)$$

2.1. GENERAL DESCRIPTION

Where $\Phi(\mathbf{r}, t)$ is the gravitational potential and G is the gravitational constant. To solve the Poisson equation we use the Fourier pseudo-spectral method, which allows for very fast numerical solutions by making use of the Fast Fourier Transform algorithm. The idea is simply to apply a Fast Fourier Transform (FFT) to the density, then solve the equation in the Fourier space, and then apply an inverse transform (IFFT). In the Fourier space the Poisson equation is given by[23] [24]

$$\lambda_{\mathbf{k}}^2 \hat{\Phi}(\mathbf{k}, t) = 4\pi G \hat{g}(\mathbf{k}, t) \quad (2.7)$$

Where $\hat{g}(\mathbf{k}, t)$ is the Fourier transform of $g(\mathbf{r}, t)$, and $\lambda_{\mathbf{k}}$ is a constant that depends on the size of the lattice and the wavevector \mathbf{k} . $\lambda_{\mathbf{k}}$ is calculated according to the approximation scheme used to solve the equation. In the the pseudo-spectral approximation, $\lambda_{\mathbf{k}}$ is given by:

$$\lambda_{\mathbf{k}}^2 = \left(\frac{2\pi k_x}{X_{max}-X_{min}} \right)^2 + \left(\frac{2\pi k_y}{Y_{max}-Y_{min}} \right)^2 + \left(\frac{2\pi k_z}{Z_{max}-Z_{min}} \right)^2 \quad (2.8)$$

Therefore, solving the Poisson equation in the Fourier space is reduced to simple arithmetic. Thanks to the highly efficient implementations of the Fast Fourier Transform Algorithm available nowadays, solving the Poisson equation takes very little time and computational resources. In this work we use the Fastest Fourier Transform of the West[25] subroutine to handle the Fast Fourier Transforms.

Once we have calculated potential, obtaining the acceleration is straight-forward:

$$\mathbf{a}(\mathbf{r}, t) = -\nabla \Phi(\mathbf{r}, t) \quad (2.9)$$

Which, in the context of the lattice can be easily calculated with a central difference

numerical derivative.

Now, in order to update the phase space, we must first define the time interval to simulate: we name N_t the number of time *instants* to simulate and dt the length of each of such instants. After calculating the acceleration and defining dt , we can update our phase space. As mentioned in section 1.5, the subtlety here is that we will only use integer arithmetic, which means that we do not exactly care about the change in velocity during a time dt but for how many cells in the phase space lattice that change represents. This is modeled by:

$$\mathbf{v}_{n+1} = \mathbf{v}_n + \lfloor \mathbf{a}_n dt \rfloor \quad (2.10)$$

With $\lfloor x \rfloor$ representing the operator “to nearest integer”, so that \mathbf{v} and $\lfloor \mathbf{adt} \rfloor$ are vectors of integers and n represents the time instant. The update of the velocity is known as “kick”. Analogously, the update of the position is known as “drift”, and is given by:

$$\mathbf{r}_{n+1} = \mathbf{r}_n + \lfloor \mathbf{v}_n dt \rfloor \quad (2.11)$$

The use of only integer arithmetics allows for the elimination of the rounding error but introduces lattice noise. Regardless, this method creates a one to one map with the continuous solution[4] [3].

The “kick” and “drift” together are known as the “Streaming” step, and it represents the classical movement of particles under a potential but without considering the collision of particles. If we want a collisionless simulation, we can just calculate again the density and continue the algorithm from there. If we want a collisional

simulation, we must define a collisional step.

2.2 The Collisional Step

As previously mentioned, solving the collisional integral $C[f]$ is not a straight-forward task, as it depends on the modeling of the short range interactions that we decide to assign to the dark matter particle. Given that the short range interaction of dark matter is unknown, we avoid using an specific description of the microscopic interactions and choose to use a mesoscopic approach instead, as discussed in section 1.6. The BGK collisional operator is given by:

$$C[f] = -\frac{1}{\tau}(f(\mathbf{r}, \mathbf{v}, t) - f_e(\mathbf{r}, \mathbf{v})) \quad (2.12)$$

Which in the context of the direct integration scheme used in the simulation becomes:

$$f(\mathbf{r} + \mathbf{v}dt, \mathbf{v}, t) = f(\mathbf{r}, \mathbf{v}, t) - \frac{dt}{\tau}(f(\mathbf{r}, \mathbf{v}, t) - f_e(\mathbf{r}, \mathbf{v})) \quad (2.13)$$

The idea behind this approach is to recover the macroscopic description of the fluid without committing to a particular microscopic description. In this scenario, the macroscopic effects of the collisions is a local relaxation towards equilibrium, which the BKG operator models using a relaxation time τ and a local equilibrium distribution $f_e(\mathbf{r}, \mathbf{v})$.

In order to implement a collisional operator we add a collisional step after the streaming step, in which the system performs a relaxation with characteristic (relaxation)

time τ towards the local equilibrium distribution $f_e(\mathbf{r}, \mathbf{v})$. It is important to notice that the BGK collisional operator is a *scattering* operator and does not consider annihilation or creation of particles.

After defining the collisional term, we have to choose a distribution function $f_e(\mathbf{r}, \mathbf{v})$. We claim that the phase space distribution relaxes towards equilibrium, which means a displacement in the phase space and not the introduction or annihilation of mass. Therefore, the equilibrium distribution must be perfectly *normalized* in order to enforce particle number conservation. We normalize this equilibrium distribution by using macroscopic quantities obtained by integrating the velocity part of the phase space. This macroscopic quantities are: the volumetric density $\rho(\mathbf{r}, t)$, the macroscopic velocity $\mathbf{u}(\mathbf{r}, \mathbf{v})$ and the internal energy $e(\mathbf{r}, \mathbf{v})$.

The volumetric density is the same density we have been using so far defined by the integral of equation 2.3. The macroscopic velocity $\mathbf{u}(\mathbf{r}, \mathbf{v})$ is defined by the integral:

$$\mathbf{u}(\mathbf{r}, \mathbf{v}) = \int_{-\infty}^{\infty} f(\mathbf{r}, \mathbf{v}, t) \mathbf{v} d\mathbf{v}. \quad (2.14)$$

When evaluating in the lattice the integral becomes:

$$\mathbf{u} = \sum_{\mathbf{v}_{min}}^{\mathbf{v}_{max}} f(\mathbf{r}, \mathbf{v}, t) \mathbf{v} d\mathbf{v} \quad (2.15)$$

And the internal energy is defined by the integral:

$$e(\mathbf{r}, \mathbf{v}) = \frac{1}{2} \int_{-\infty}^{\infty} f(\mathbf{r}, \mathbf{v}, t) (\mathbf{v} - \mathbf{u})^2 d\mathbf{v}. \quad (2.16)$$

2.2. THE COLLISIONAL STEP

Which also becomes a sum when evaluating in the lattice:

$$e(\mathbf{r}, \mathbf{v}) = \frac{1}{2} \sum_{\mathbf{v}_{min}}^{\mathbf{v}_{max}} f(\mathbf{r}, \mathbf{v}, t) (\mathbf{v} - \mathbf{u})^2 d\mathbf{v} \quad (2.17)$$

Note that we are not including explicitly the mass of the dark matter particle in this integrals because it has already been included in the phase space definition.

Now that we have well defined macroscopic variables, we can proceed to choose an equilibrium distribution. Such distribution must obey the next condition:

$$C[f_e] = 0 \quad (2.18)$$

Which simply means that if the system is already in local equilibrium, then there is no relaxation. This condition can also be stated as “the equilibrium function must be a collisional invariant”. In order for $f_e(\mathbf{r}, \mathbf{v})$ to be a collisional invariant, it must be build with variables that are also collisional invariant. Fortunately, the macroscopic variables already defined in this chapter are also collisional invariants, and so, we can use them to build equilibrium distributions. The idea behind normalization is to obtain the same macroscopic variables when integrating over $f_e(\mathbf{r}, \mathbf{v})$ instead of $f(\mathbf{r}, \mathbf{v}, t)$. In this work we use distributions based on the Maxwell-Boltzmann velocity distribution. Alternative equilibrium distributions functions can be considered and may be of interest, but they are beyond the scope of this work. In particular, quantum Maxwellians may be used to include annihilation and creation of particles, and the effects of Bose-Einstein, Fermi-Dirac statistics[22].

The equilibrium function to use is a classical Maxwellian properly normalized for the case of interest:

$$f_e(\mathbf{r}, \mathbf{v}) = \frac{\rho}{[2\pi e(\mathbf{r}, \mathbf{v})]^{D/2}} \exp\left[-\frac{(\mathbf{v} - \mathbf{u})^2}{2 e(\mathbf{r}, \mathbf{v})}\right] \quad (2.19)$$

Where D is the number of spatial dimensions. For example, if the system is a three dimensional dark matter halo, then D will be equal to three. The Maxwell distribution was originally used to describe the probability distribution of the velocity in a gas under kinetic theory assumptions. Here, we assume collisions as a phenomena that happens instantly. During the time in between, the mechanics of the system are governed by the self-gravitational potential. Therefore, the Maxwell distribution is a good ansatz for the collisional equilibrium distribution function $f_e(\mathbf{r}, \mathbf{v})$.

Finally, we only need to choose a relaxation time. As in classic kinetic theory, our relaxation time will be given by:

$$\tau = \frac{1}{n < \sigma v >} \quad (2.20)$$

In terms of the matter density instead of particle number:

$$\tau = \frac{m}{\rho < \sigma v >} \quad (2.21)$$

With n being the mean particle number in the halo, m being the mass of a dark matter particle, ρ being the average density of a dark matter halo and $< \sigma v >$ is the thermally averaged cross-section of the particle.

For this simulation we use the average *matter* density of the universe, given by the most recent results of the Planck probe[26]. We are also going to use the value of $< \sigma v >$ constrained by the Bullet Cluster data [27] [28], and for the dark particle

2.2. THE COLLISIONAL STEP

mass we are going to use the lowest mass possible for a fermionic dark matter particle candidate [18]. These values are:

$$m = 0.7\text{KeV} \quad (2.22)$$

$$\langle \sigma v \rangle = 3 \times 10^{-26}\text{cm}^3/\text{s} \quad (2.23)$$

$$\rho = \Omega_m = 0.312 \quad (2.24)$$

The final value of τ will depend on the particular set of units used in every scenario.

2.2.1 Units on the simulation

To set the units we fix the value of one spatial unit (us), one unit of time (ut), and one unit of mass (um) of the simulation, and from there, we proceed to calculate the values of the physical constants in our units. The physical constant of interest here is the gravitational constant, since it gives the coupling of the gravitational interaction. We chose units to simulate a dark matter halo of dimensions akin to the Milky Way's dark matter halo. Because of stability conditions, the units may differ between runs, therefore, they are specified at the beginning of each section in the next chapter.

Chapter 3

Results

For the development of this work we wrote and ran three simulations: a two dimensional phase space simulation (one spatial and one velocity dimension), a four dimensional phase space simulation, and a six dimensional phase space simulation. The first one was developed in order to reproduce the results of Philip Mocz and Sauro Succi published in 2016 [3], and the results of Sebastian Franco published in 2017 [4]. In addition to reproducing results, we also extended the simulation to account for a collisional operator and tested it with different initial conditions.

The four dimensional simulation was developed as a step to develop the six dimensional simulation. Developing a four dimensional simulation allows to implement and test the specifics of increasing dimensionality without much of the visualization problems that arise from a six dimensional simulation.

The six dimensional simulation is one of the main scopes of this work. The simulation was implemented successfully, however, due to the high RAM memory requirements

of the Lattice-Boltzmann method, the resolution is heavily constrained. Even using the HPC cluster available at “Universidad de los Andes”, the resolution of the simulation was too poor to reproduce the results from the other two simulations.

3.1 The two dimensional phase space

For the two dimensional simulation we only need two axes, which allows for a very high resolution. We used an squared grid characterized by:

$$W_{min} = -1 \quad (3.1)$$

$$W_{max} = 1 \quad (3.2)$$

$$N_w = 2048 \quad (3.3)$$

$$dw = 1/1024 \quad (3.4)$$

As mentioned in section 2.1, W represents the axis (in this case r or v), N_w represents the size of the grid in the w axis, dw represents the size of a lattice unit in the w axis and -1 and 1 are the extremal values of the phase space in the w axis. We always use grid sizes of the form $N_w = 2^n$ with n positive integer, because the Fast Fourier Transform algorithm performs better and faster when calculating discrete transforms of sizes $2^n 3^m 5^l$ for n,m,l positive integers.

In this section we are going to use three initial conditions:

- A Gaussian density profile used to test the code, and explain the expected behaviors of the phase space density time-evolution.

- A Jeans instability test, in which we reproduce the spatial conditions for a periodic jeans oscillation and use a Gaussian profile for the velocity distribution. These conditions are used to reproduce the previous work aforementioned.
- A Bullet Cluster-like initial conditions, in which we have two Gaussian profiles (each one with its own variance and amplitude) separated by a given distance. One of the main scopes of this work is to analyze the Bullet Cluster-like system and compare the phase space evolution of the collisional case its collisionless counterpart. Additionally, we are going to reproduce the behavior of the collisional baryonic gas.

3.1.1 No collisional case

We begin with the Gaussian conditions because their simplicity and ease to analyze makes them the best introductory example. The initialization of the phase space can be seen in figure 3.1, along with its correspondent spatial density. After initialization we proceed to calculate the potential and the acceleration, which can be seen in figure 3.2. The values used to initialize the phase space were:

$$\sigma_r = 0.2 \text{ us} \quad (3.5)$$

$$\sigma_v = 0.2 \text{ us/ut} \quad (3.6)$$

$$A = 50 \text{ um} \quad (3.7)$$

Which yields a total mass of $1.26 \times 10^{12} M_\odot$, a value in accordance with recent estimates of the total mass of our galaxy's dark matter halo [29].

3.1. THE TWO DIMENSIONAL PHASE SPACE

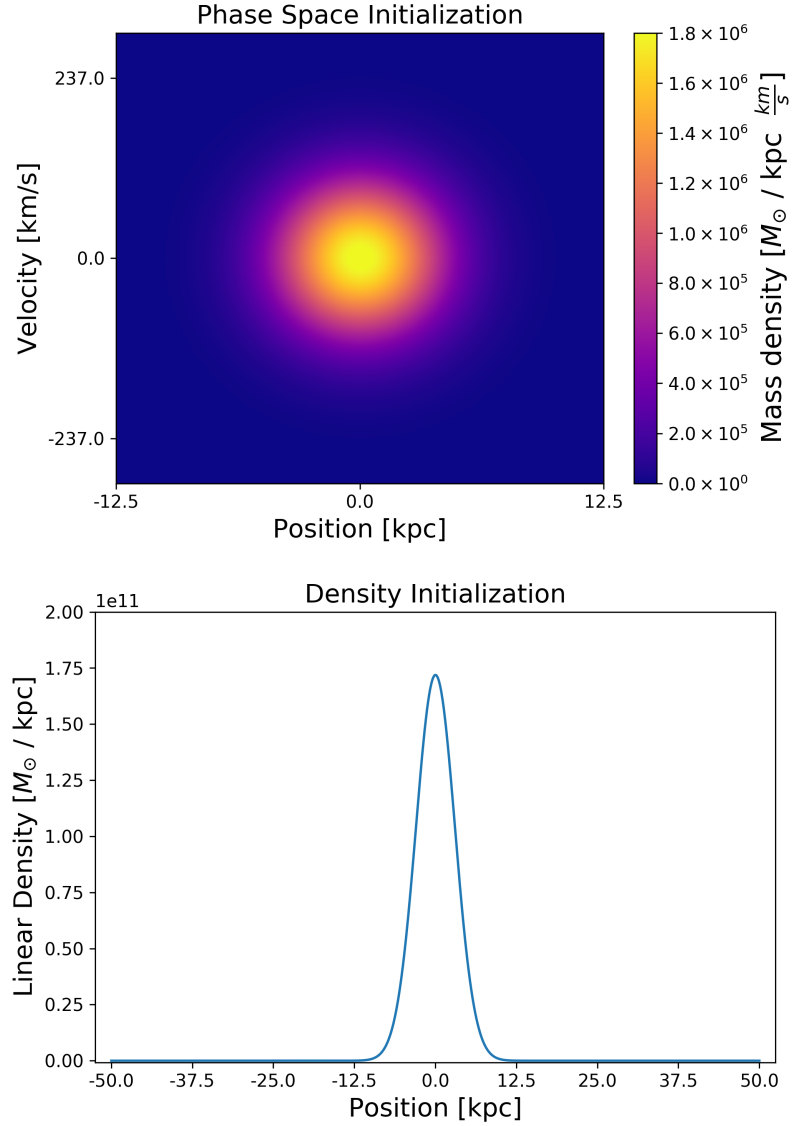


Figure 3.1: Up: initialization of the phase space. Position is represented in the x axis, and velocity in the y axis of the plot. Down: the spatial density obtained through integration.

To test the simulation we reproduce previous work in the collisionless case. For which we run the simulation and check upon the behavior of the phase space density,

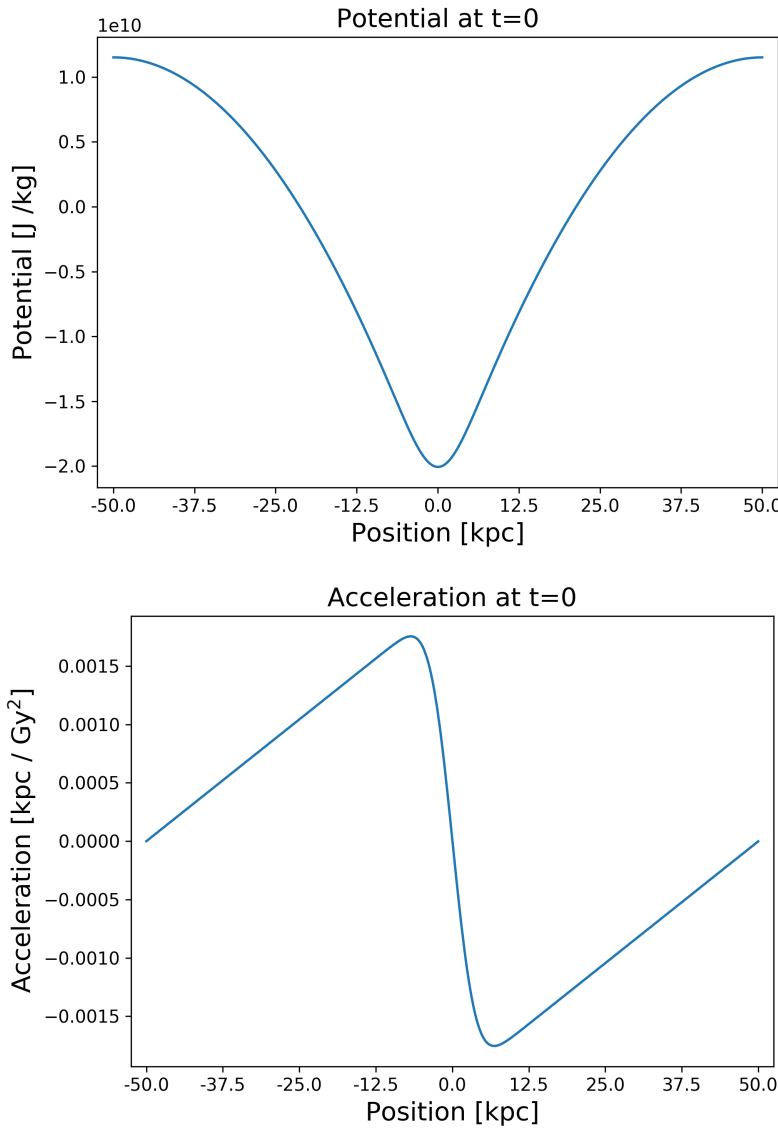


Figure 3.2: Up: The potential obtained by solving the Poisson equation. Given that the density was a Gaussian profile, it is no surprise that the potential is a negative Gaussian profile. Down: The acceleration obtain by numerical derivation of the potential.

3.1. THE TWO DIMENSIONAL PHASE SPACE

the spatial density, the potential and the acceleration. In the phase space grid, we expect the cells with positive velocity to move to the right side of the plot, but, as they move to the right they are also being attracted towards the left because of the symmetry of the initial conditions. Therefore, the cells with positive velocity will move towards the inferior-right side of the plot, while cells with negative velocity will move towards the upper left side of the phase space.

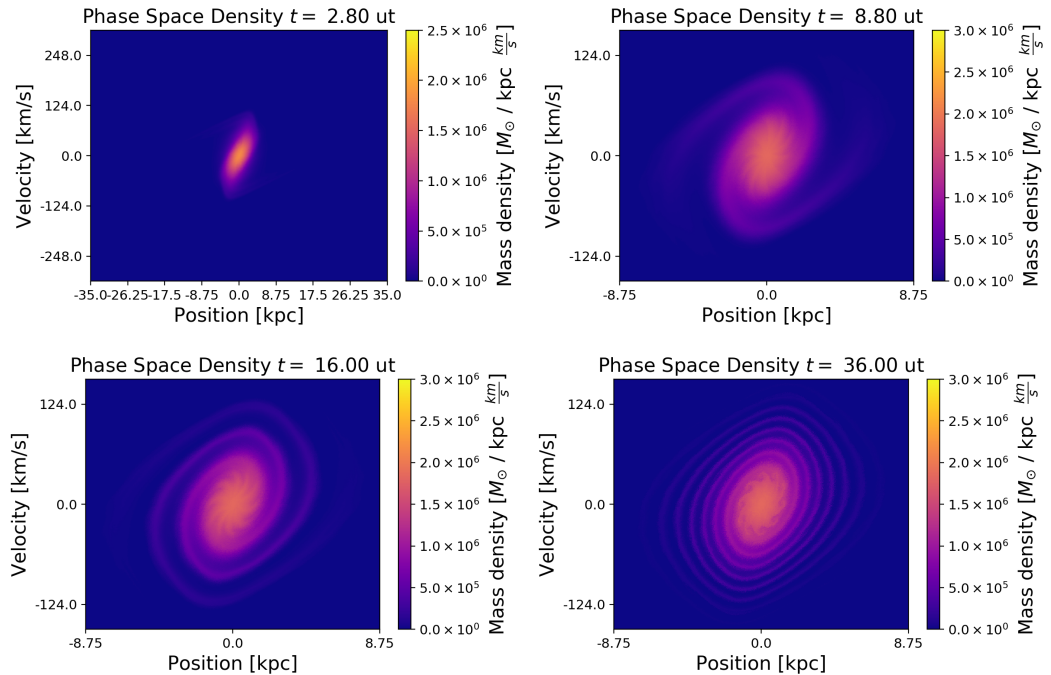


Figure 3.3: Upper left: Phase space 72 million years after initialization. Upper right: Phase space 227 million years after initialization. Bottom left: Phase space 413 million years after initialization. Bottom right: Phase space 930 million years after initialization. It can be observed that the phase space behaves as a clock-wise rotating spiral.

This behavior is in complete accordance with previous work and can be seen in figure 3.3, where we plot different time instants chosen to display the clock-wise spiral of the phase space evolution.

To visualize the linear density, we plot the linear density vs position. We observe an initial increase in the height of the central peak and then little bumps trying to abandon the central distribution but they are gravitationally pulled back before crossing the spatial of the lattice boundaries. This behavior can be seen in figure 3.4

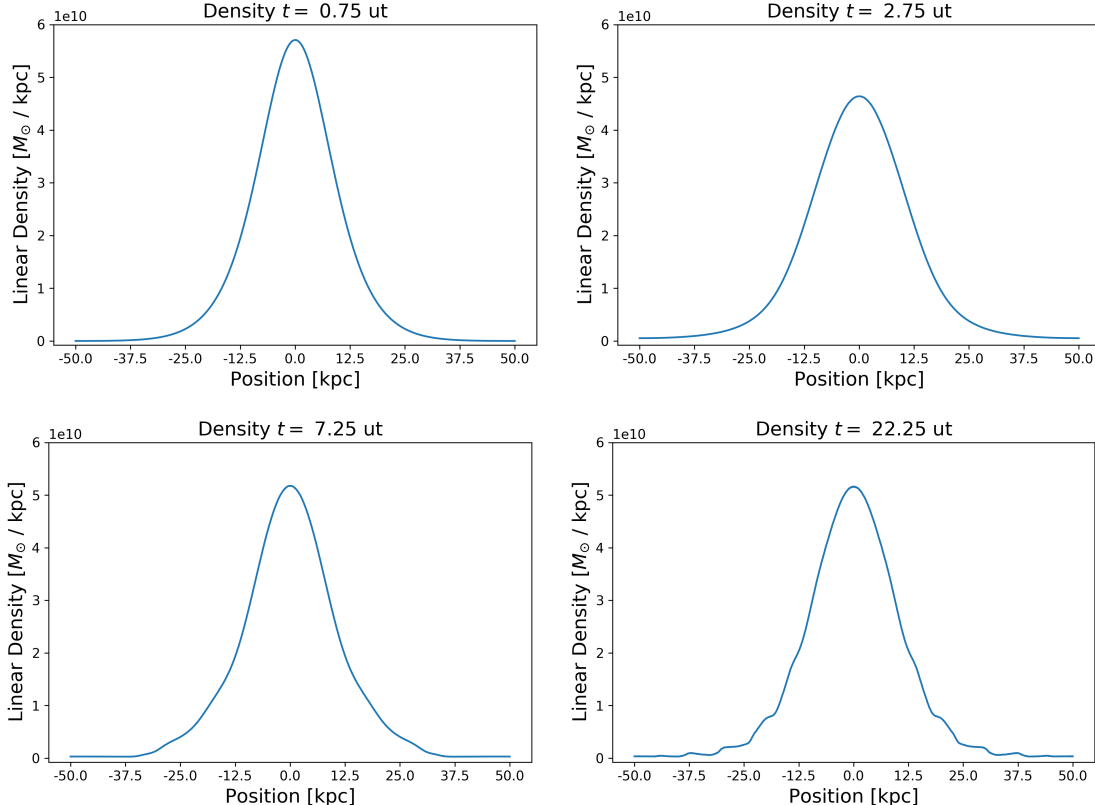


Figure 3.4: Upper left: linear density with its central peak at maximum height. Upper right: linear density the peak at a local minima after having reached maximum height . Bottom left: little bumps can be seen at the tails of the distribution. Bottom right: the tails of the distribution are completely bumpy and so is the base of the peak. The images are from 31, 114, 300 and 920 million years after initialization.

In addition to Gaussian initial conditions, we reproduced the Jeans instability, which

3.1. THE TWO DIMENSIONAL PHASE SPACE

was also tested in previous work. In this scenario, the Jeans instability is given by:

$$f(r, v, 0) = \frac{\bar{\rho}}{(2\pi\sigma^2)^{1/2}} \exp\left(-\frac{v^2}{2\sigma^2}\right) (1 + A \cos(kr)) \quad (3.8)$$

Such that $\bar{\rho}$ is the average phase density of the system, σ is a measure of the width of the velocity Gaussian profile, A is the amplitude of the density fluctuation and k is the wavenumber of the density fluctuation. We used the following values:

$$\bar{\rho} = 10 \text{ um us}^{-1} (\text{us}/\text{ut})^{-1} \quad (3.9)$$

$$\sigma = 0.1 \text{ us}/\text{ut} \quad (3.10)$$

$$A = 0.9999 \quad (3.11)$$

$$k = 2\pi \text{ us}^{-1} \quad (3.12)$$

For which the phase space behaved like three successive Gaussian profiles, that is because we met the Jeans instability criteria. This result were also compatible with previous work published on one dimensional collisionless dark matter fluids. The evolution of the Jeans instability phase space can be seen in figure 3.5

The last set of initial conditions is the Bullet Cluster-like scenario, in which two Gaussian distributions of mass collide due to their gravitational interaction. Each Gaussian has its own variance and amplitude. Reminiscent of the Bullet Cluster's conditions before the collision, we fix the mass of one halo greater than the other.

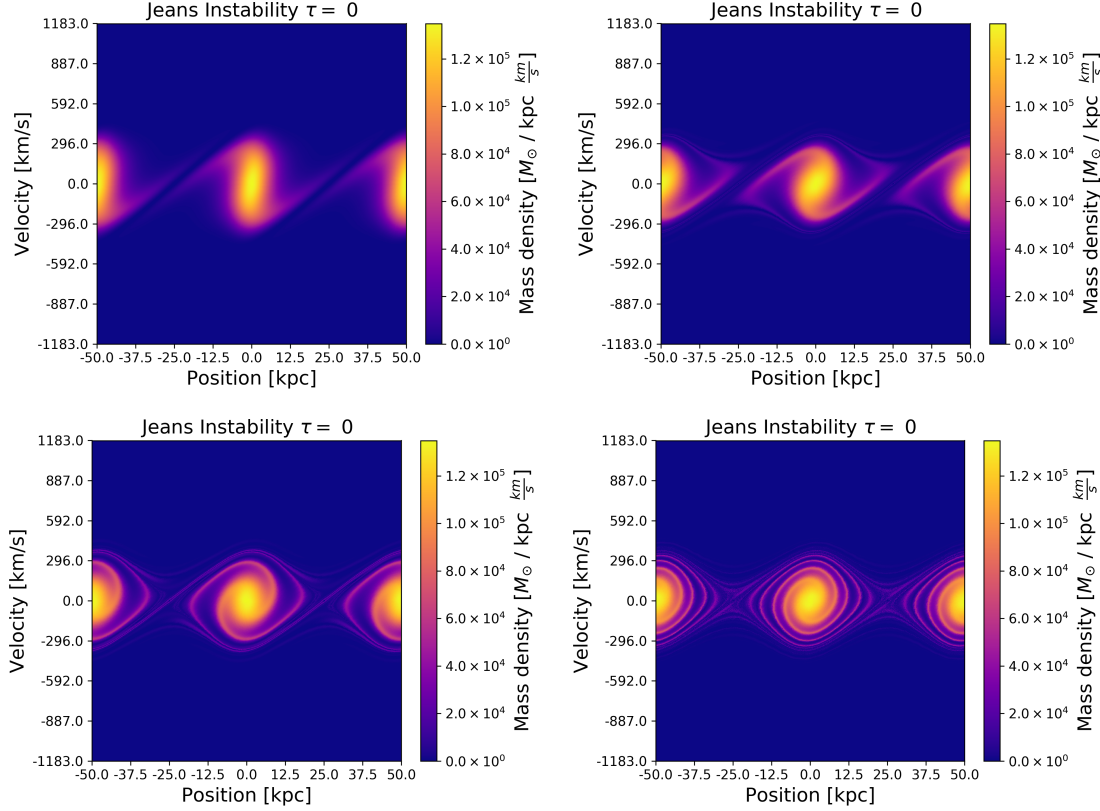


Figure 3.5: Upper left: Phase space 72 million years after initialization. Upper right: Phase space 227 million years after initialization. Bottom left: Phase space 413 million years after initialization. Bottom right: Phase space 930 million years after initialization. The behavior is the same as three successive Gaussian conditions.

The initial conditions are given by the distribution:

$$f(\mathbf{r}, \mathbf{v}, 0) = A_1 \exp\left\{-\frac{(x - 0.4)^2}{2\sigma_1^2} - \frac{v^2}{2\sigma_v^2}\right\} + A_2 \exp\left\{-\frac{(x + 0.4)^2}{2\sigma_2^2} - \frac{v^2}{2\sigma_v^2}\right\} \quad (3.13)$$

Such that A_i is a measure of the total mass of the i th halo, σ_i^2 is the variance of the Gaussian profile of the halo in the spatial axis, and σ_v^2 is the variance of the Gaussian

3.1. THE TWO DIMENSIONAL PHASE SPACE

profile in the velocity axis. The values used to initialize the simulation were:

$$\sigma_1 = 0.04 \text{ us} \quad (3.14)$$

$$\sigma_2 = 0.04 \text{ us} \quad (3.15)$$

$$\sigma_v = 0.06 \text{ us} \quad (3.16)$$

$$A_1 = 40 \text{ um} \quad (3.17)$$

$$A_2 = 30 \text{ um} \quad (3.18)$$

Given the collisionless nature of this run, we expect the halos to simply pass through each other *without any loss of energy* due to the collision. In other words, the *density* profiles will have a periodic movement and will eventually return to their initial position. In the phase space we will see that each halo forms the counter-clockwise spiral from the Gaussian initial conditions. In addition to that, we can see how when the clusters occupy the same spatial position, they have very different velocities, which keeps them decoupled. The evolution of the phase space can be seen in figure 3.6. The oscillations in the spatial density can be seen in figure 3.7

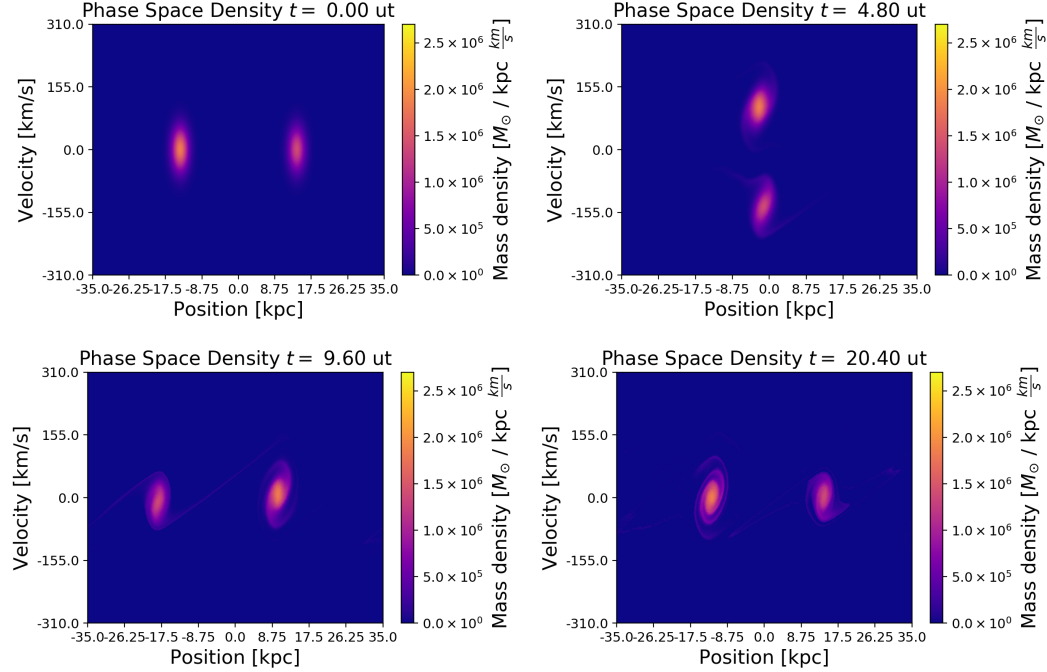


Figure 3.6: Upper left: phase space initialization of the *Bullet Cluster* run. The right halo is slightly less massive (darker). Upper right: phase space during the spatial collision of the halos. The gap in the velocity axis keeps the halos decoupled. Bottom left: phase space with the position of the halos switched in regards of the centre of mass and the initial conditions. Bottom right: the system after a full period. The halos are at their initial position but their velocities have changed due to the evolution of each Gaussian.

3.1.2 The collisional case

Now, for the collisional case we are going to repeat the same initial conditions and evolve them. Recalling the discussion on choosing a τ (see 2.2), the final value was unit dependent. The value of τ in the units used in this section is

$$\tau = 8972$$

3.1. THE TWO DIMENSIONAL PHASE SPACE

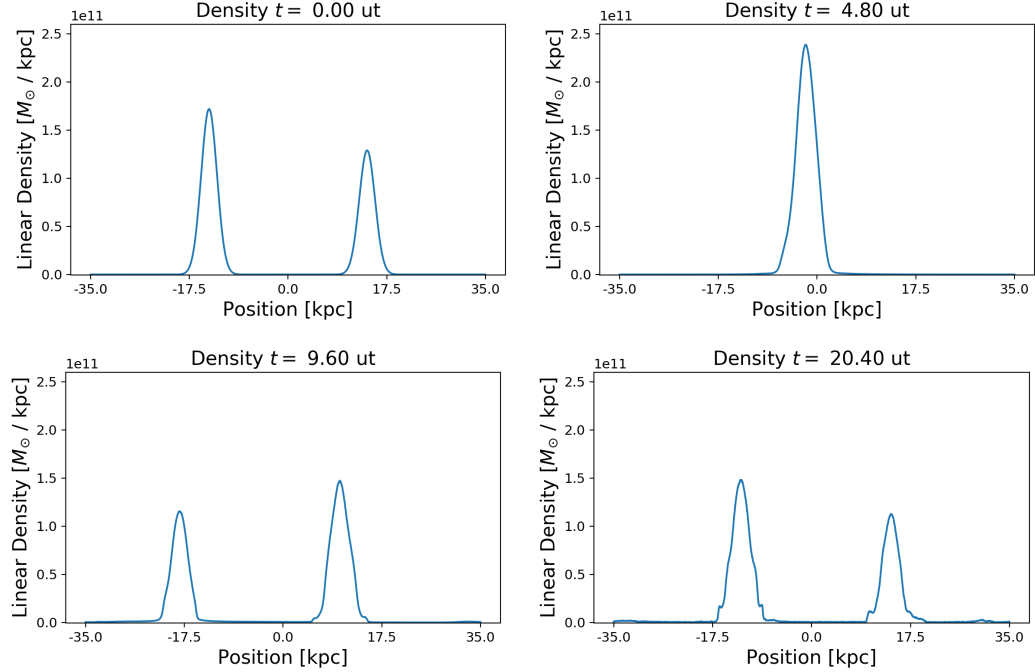


Figure 3.7: Upper left: density initialization of the *Bullet Cluster* run. Notice that the left halo is heavier. Upper right: density during the spatial collision of the halos. Bottom left: density when the halos have switched position with regards to the centre of mass. Bottom right: the system after a full period. The halos are at their initial position but their velocities have changed.

Once again, we start with the Gaussian initial conditions. We ran the simulation with exactly the same initial conditions and observed the behavior in phase space. The value of τ implies a very little collisional term, therefore, the difference in the phase space evolution of the Gaussian distribution can not be seen by eye. Instead, we plot the porcentual difference, defined by:

$$Z = 100 \left(\frac{f_\tau(\mathbf{r}, \mathbf{v}, t) - f_0(\mathbf{r}, \mathbf{v}, t)}{f_0(\mathbf{r}, \mathbf{v}, t)} \right) \quad (3.19)$$

Which will allow us to

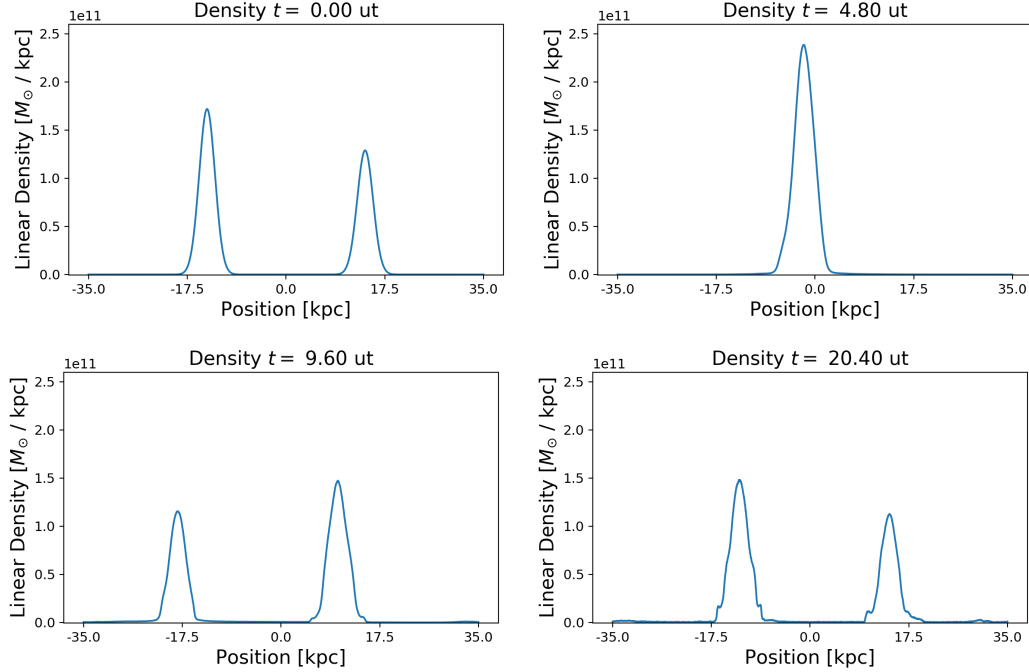


Figure 3.8: Upper left: density initialization of the *Bullet Cluster* run. Notice that the left halo is heavier. Upper right: density during the spatial collision of the halos. Bottom left: density when the halos have switched position with regards to the centre of mass. Bottom right: the system after a full period. The halos are at their initial position but their velocities have changed.

3.2 Four dimensional phase space

In the case of the four dimensional phase space we need four axes to describe the phase space. This increase in the number of axes in regards to the two dimensional case means that we are going to have to sacrifice a lot of resolution in order to comply

3.2. FOUR DIMENSIONAL PHASE SPACE

to RAM memory constrains. The four dimensional grid used is characterized by:

$$W_{min} = -1 \quad (3.20)$$

$$W_{max} = 1 \quad (3.21)$$

$$N_w = 128 \quad (3.22)$$

$$dw = 1/64 \quad (3.23)$$

Likewise, the of units to use are:

$$1 \text{ } us = 50 \text{ kpc} \quad (3.24)$$

$$1 \text{ } ut = 0.003 \text{ } t_0 \quad (3.25)$$

$$1 \text{ } um = 10^{11} \text{ } M_\odot \quad (3.26)$$

With t_0 being the age of the universe today, M_\odot being a solar mass and a kiloparsec (kpc) is equal to 3.0857×10^{19} m. In this units, the gravitational constant has a value of:

$$G = 0.006141 \text{ } (1 \text{ } us)^3 \text{ } (1 \text{ } um)^{-1} \text{ } (1 \text{ } ut)^{-2} \quad (3.27)$$

3.2.1 No collisional case

The four dimensional case is initialized using a Gaussian distribution.

3.3 Six dimensional phase space

Chapter 4

Conclusions

4.1 A Numerically Stable Simulation

Bibliography

- [1] M. Kuhlen, M. Vogelsberger, and R. Angulo. Numerical simulations of the dark universe: State of the art and the next decade. *Physics of the Dark Universe*, 1:50–93, November 2012.
- [2] M. Davis, G. Efstathiou, C. S. Frenk, and S. D. M. White. The evolution of large-scale structure in a universe dominated by cold dark matter. 292:371–394, May 1985.
- [3] Philip Mocz and Sauro Succi. Integer lattice dynamics for Vlasov–Poisson. *Mon. Not. Roy. Astron. Soc.*, 465(3):3154–3162, 2017.
- [4] Sebastián Franco Ulloa. Simulaciones de un fluido débilmente auto-interactuante con métodos de lattice-boltzmann. Master’s thesis, Universidad de los Andes, 5 2017.
- [5] Planck Collaboration, P. A. R. Ade, N. Aghanim, C. Armitage-Caplan, M. Arnaud, M. Ashdown, F. Atrio-Barandela, J. Aumont, C. Baccigalupi, A. J. Banday, and et al. Planck 2013 results. XVI. Cosmological parameters. 571:A16, November 2014.

BIBLIOGRAPHY

- [6] Gianfranco Bertone and Dan Hooper. A History of Dark Matter. *Submitted to: Rev. Mod. Phys.*, 2016.
- [7] J. M. Cline. TASI Lectures on Early Universe Cosmology: Inflation, Baryogenesis and Dark Matter. *ArXiv e-prints*, July 2018.
- [8] H. Andernach and F. Zwicky. English and Spanish Translation of Zwicky's (1933) The Redshift of Extragalactic Nebulae. *ArXiv e-prints*, November 2017.
- [9] M. Schwarzschild. Mass distribution and mass-luminosity ratio in galaxies. 59:273, September 1954.
- [10] Meekins J. F., Fritz G., Chubb T. A., and Friedman H. Physical Sciences: X-rays from the Coma Cluster of Galaxies. 231:107–108, May 1971.
- [11] A. Penzias. Free Hydrogen in the Pegasus I Cluster of Galaxies. 66:293, March 1961.
- [12] I S. Chandrasekhar. The time of relaxation of stellar systems. 93:285, 02 1941.
- [13] D. H. Rogstad and G. S. Shostak. Gross Properties of Five Scd Galaxies as Determined from 21-CENTIMETER Observations. 176:315, September 1972.
- [14] M. S. Roberts and R. N. Whitehurst. The rotation curve and geometry of M31 at large galactocentric distances. 201:327–346, October 1975.
- [15] V. C. Rubin and W. K. Ford, Jr. Rotation of the Andromeda Nebula from a Spectroscopic Survey of Emission Regions. 159:379, February 1970.

- [16] J. P. Ostriker, P. J. E. Peebles, and A. Yahil. The size and mass of galaxies, and the mass of the universe. 193:L1–L4, October 1974.
- [17] J. F. Navarro, C. S. Frenk, and S. D. M. White. The Structure of Cold Dark Matter Halos. 462:563, May 1996.
- [18] Mariangela Lisanti. Lectures on Dark Matter Physics. In *Proceedings, Theoretical Advanced Study Institute in Elementary Particle Physics: New Frontiers in Fields and Strings (TASI 2015): Boulder, CO, USA, June 1-26, 2015*, pages 399–446, 2017.
- [19] John S. Gallagher III Linda S. Sparke. *Galaxies in the Universe: An Introduction*. Cambridge University Press, 2 edition, 2007.
- [20] P. L. Bhatnagar, E. P. Gross, and M. Krook. A Model for Collision Processes in Gases. I. Small Amplitude Processes in Charged and Neutral One-Component Systems. *Physical Review*, 94:511–525, May 1954.
- [21] Prieto Asinari. *Multi-Scale Analysis of Heat and Mass Transfer in Mini/Micro-Structures*. PhD thesis, Politecnico di Torino, 2005.
- [22] F. Filbet, J. Hu, and S. Jin. A Numerical Scheme for the Quantum Boltzmann Equation Efficient in the Fluid Regime. *ArXiv e-prints*, September 2010.
- [23] V. Fuka. PoisFFT - A Free Parallel Fast Poisson Solver. *ArXiv e-prints*, September 2014.
- [24] J.W Eastwood R.W Hockney. *Computer simulation using particles*.

BIBLIOGRAPHY

- [25] Matteo Frigo and Steven G. Johnson. The design and implementation of FFTW3. *Proceedings of the IEEE*, 93(2):216–231, 2005. Special issue on “Program Generation, Optimization, and Platform Adaptation”.
- [26] Planck Collaboration, N. Aghanim, Y. Akrami, M. Ashdown, J. Aumont, C. Baccigalupi, M. Ballardini, A. J. Banday, R. B. Barreiro, N. Bartolo, S. Basak, R. Battye, K. Benabed, J.-P. Bernard, M. Bersanelli, P. Bielewicz, J. J. Bock, J. R. Bond, J. Borrill, F. R. Bouchet, F. Boulanger, M. Bucher, C. Burigana, R. C. Butler, E. Calabrese, J.-F. Cardoso, J. Carron, A. Challinor, H. C. Chiang, J. Chluba, L. P. L. Colombo, C. Combet, D. Contreras, B. P. Crill, F. Cuttaia, P. de Bernardis, G. de Zotti, J. Delabrouille, J.-M. Delouis, E. Di Valentino, J. M. Diego, O. Doré, M. Douspis, A. Ducout, X. Dupac, S. Dusini, G. Efstathiou, F. Elsner, T. A. Enßlin, H. K. Eriksen, Y. Fantaye, M. Farhang, J. Fergusson, R. Fernandez-Cobos, F. Finelli, F. Forastieri, M. Frailis, E. Franceschi, A. Frolov, S. Galeotta, S. Galli, K. Ganga, R. T. Génova-Santos, M. Gerbino, T. Ghosh, J. González-Nuevo, K. M. Górski, S. Gratton, A. Gruppuso, J. E. Gudmundsson, J. Hamann, W. Handley, D. Herlitz, E. Hivon, Z. Huang, A. H. Jaffe, W. C. Jones, A. Karakci, E. Keihänen, R. Keskitalo, K. Kiiveri, J. Kim, T. S. Kisner, L. Knox, N. Krachmalnicoff, M. Kunz, H. Kurki-Suonio, G. Lagache, J.-M. Lamarre, A. Lasenby, M. Latanzi, C. R. Lawrence, M. Le Jeune, P. Lemos, J. Lesgourgues, F. Levrier, A. Lewis, M. Liguori, P. B. Lilje, M. Lilley, V. Lindholm, M. López-Caniego, P. M. Lubin, Y.-Z. Ma, J. F. Macías-Pérez, G. Maggio, D. Maino, N. Mandlesi, A. Mangilli, A. Marcos-Caballero, M. Maris, P. G. Martin, M. Martinelli, E. Martínez-González, S. Matarrese, N. Mauri, J. D. McEwen, P. R. Meinhold, A. Melchiorri, A. Mennella, M. Migliaccio, M. Millea, S. Mitra, M.-A. Miville-

- Deschênes, D. Molinari, L. Montier, G. Morgante, A. Moss, P. Natoli, H. U. Nørgaard-Nielsen, L. Pagano, D. Paoletti, B. Partridge, G. Patanchon, H. V. Peiris, F. Perrotta, V. Pettorino, F. Piacentini, L. Polastri, G. Polenta, J.-L. Puget, J. P. Rachen, M. Reinecke, M. Remazeilles, A. Renzi, G. Rocha, C. Rosset, G. Roudier, J. A. Rubiño-Martín, B. Ruiz-Granados, L. Salvati, M. Sandri, M. Savelainen, D. Scott, E. P. S. Shellard, C. Sirignano, G. Sirri, L. D. Spencer, R. Sunyaev, A.-S. Suur-Uski, J. A. Tauber, D. Tavagnacco, M. Tenti, L. Toffolatti, M. Tomasi, T. Trombetti, L. Valenziano, J. Valiviita, B. Van Tent, L. Vibert, P. Vielva, F. Villa, N. Vittorio, B. D. Wandelt, I. K. Wehus, M. White, S. D. M. White, A. Zacchei, and A. Zonca. Planck 2018 results. VI. Cosmological parameters. *ArXiv e-prints*, July 2018.
- [27] S. W. Randall, M. Markevitch, D. Clowe, A. H. Gonzalez, and M. Bradač. Constraints on the Self-Interaction Cross Section of Dark Matter from Numerical Simulations of the Merging Galaxy Cluster 1E 0657-56. *679*:1173–1180, June 2008.
- [28] A. Robertson, R. Massey, and V. Eke. What does the Bullet Cluster tell us about self-interacting dark matter? *465*:569–587, February 2017.
- [29] F. Nesti and P. Salucci. The Dark Matter halo of the Milky Way, AD 2013. 7:016, July 2013.
- [30] P. A. R. Ade et al. Planck 2013 results. I. Overview of products and scientific results. *Astron. Astrophys.*, 571:A1, 2014.
- [31] P. Gondolo and G. Gelmini. Cosmic abundances of stable particles: improved analysis. *Nuclear Physics B*, 360:145–179, August 1991.

BIBLIOGRAPHY

- [32] Dr Jian Guo Zhou. *Lattice Boltzmann Method*. 01 2004.
- [33] Andrew Liddle. *An Introduction to Modern Cosmology*. Wiley, 2nd ed edition, 2003.
- [34] Aleksei Parnowski Serge Parnovsky. *How the Universe Works: Introduction to Modern Cosmology*. World Scientific Publishing, 2018.
- [35] M. Xiaochun, X. Kuan, and Y. Ping. The Calculations of Gravity Fields and Rotation Curves of Whirlpool Galaxies and Dark Material. *ArXiv e-prints*, March 2009.
- [36] Frederick Reif. *Fundamentals of statistical and thermal physics*. McGraw-Hill Series in Fundamentals of Physics. McGraw-Hill Science/Engineering/Math, 1 edition, 1965.
- [37] Ostlie D.A. Carroll B.W. *An introduction to modern astrophysics*. 2ed., pearson edition, 2007.